

# Design and Control of a MEMS Nanopositioner with Bulk Piezoresistive Sensors

Mohammad Maroufi, Y. K. Yong<sup>1</sup> and S. O. Reza Moheimani<sup>2</sup>

**Abstract**—A 2 degree of freedom microelectromechanical system (MEMS) nanopositioner is presented in this paper. The nanopositioner is fabricated using a standard silicon-on-insulator process. The device demonstrates a bidirectional displacement in two orthogonal directions. As the displacement sensing mechanism, bulk piezoresistivity of tilted clamped-guided beams is exploited. The characterization reveals more than 15  $\mu\text{m}$  displacement range and an in-plane bandwidth of above 3.6 kHz in both axes. The piezoresistive sensors provide a bandwidth which is more than ten times larger than the stage's resonant frequency. To evaluate the sensor performance in closed-loop, an integral resonant controller together with an integral tracking controller are implemented where piezoresistive sensor outputs are used as measurement. The controlled nanopositioner is used for imaging in an atomic force microscope.

## I. INTRODUCTION

The invaluable feature of nanopositioners for producing displacements with nanometer and sub-nanometer resolution made these devices a crucial instrument for numerous state-of-the-art applications. Nanolithography [1], scanning probe microscopy [2] and probe data storage systems with ultrahigh density [3] are among the example of such applications.

Recently, the microelectromechanical system (MEMS) nanopositioners have also found applications as scanners in on-chip atomic force microscopes (AFM) [4] and probe data storage systems [5].

For realization of MEMS nanopositioner, a range of actuation and sensing mechanisms can be used. As actuators, electrostatic and electrothermal actuation mechanisms are more prevalent. In comparison with electrostatic actuators, electrothermal actuators provide a relatively high force. However, their sluggish dynamics, due to the involvement of heat transfer mechanism, limits their use in high-speed MEMS nanopositioners.

Displacement sensing mechanisms such as capacitive [6], electrothermal [7] and piezoresistive [8] can be incorporated in MEMS devices. The capacitive sensing mechanism, in particular, is predominately used in MEMS nanopositioners (for example see [9]–[11]). The implementation of capacitive sensors is often compatible with standard microfabrication processes and they typically demonstrate a high-resolution

performance in a wide bandwidth. However, using this sensing mechanism typically necessitates the allocation of a part of nanopositioners' mechanical structure to the sensing capacitors, which leads to an occupation of an extra area of the chip. In addition, a relatively complex readout circuit is needed to detect small capacitance changes at the presence of parasitic capacitors [12].

The electrothermal sensors typically comprise a pair of heaters and a stage which functions as a heat sink. The displacement is measured based on the temperature variations and, as a result, opposite resistance changes in the pair of heaters induced by the stage displacement [13], [14]. Small form factor and the requirement of a relatively simple readout circuit are among the benefits of utilizing this sensor. Electrothermal sensors are also implemented in MEMS nanopositioners [4], [15]. However, their limited bandwidth poses a restriction on the achievable scanning speed of the MEMS nanopositioner.

Piezoresistivity of silicon, which is the variation of its electrical conductivity under mechanical stress, has also been exploited as sensing mechanism in MEMS nanopositioners [8], [16]. These displacement sensors are normally realized by implementing heavily doped areas on high-stressed zones of silicon flexures. These sensors require relatively simple readout circuitry and, in contrast to the electrothermal sensors, offer a wide sensing bandwidth. The implementation of the piezoresistive sensors, however, requires additional and often non-standard fabrication steps which hinders their widespread application.

To address the implementation problem, we proposed a novel piezoresistive displacement sensor in [17], which excluded the need for additional fabrication and doping steps. In that design, the bulk piezoresistivity of entire structure of a pair of tilted beams was exploited rather than some heavily doped small zones. In addition, the mechanical structure was designed such that the sensors operates differentially.

In this paper, a 2-DOF MEMS nanopositioner with the tilted beam piezoresistors is proposed to be incorporated as a scanner within an AFM. The titled beams also function as a part of the device's suspension system, so the space allocated to this sensing mechanism is practically zero. For the implementation, the standard SOIMUMPs process is used [18]. The characterization reveals a relatively large displacement range and mechanical bandwidth. By a proper design, the bandwidth of displacement sensors is also enhanced. Thus, the sensors completely capture the device dynamics in a frequency range which is ten times larger than the first mechanical resonant mode. The static and dynamic

\*This work is supported by Australian research council (ARC).

<sup>1</sup>Mohammad Maroufi and Y. K. Yong are with the School of Electrical Engineering and Computer Science, University of Newcastle, Callaghan, NSW 2308, Australia, Mohammad.Maroufi@uon.edu.au, Yuenkuan.Yong@newcastle.edu.au

<sup>2</sup>S. O. Reza Moheimani was with the School of Electrical Engineering and Computer Science, University of Newcastle, Australia. He is now with the Department of Mechanical Engineering, the University of Texas at Dallas, Richardson, TX 75080, USA, Reza.Moheimani@utdallas.edu

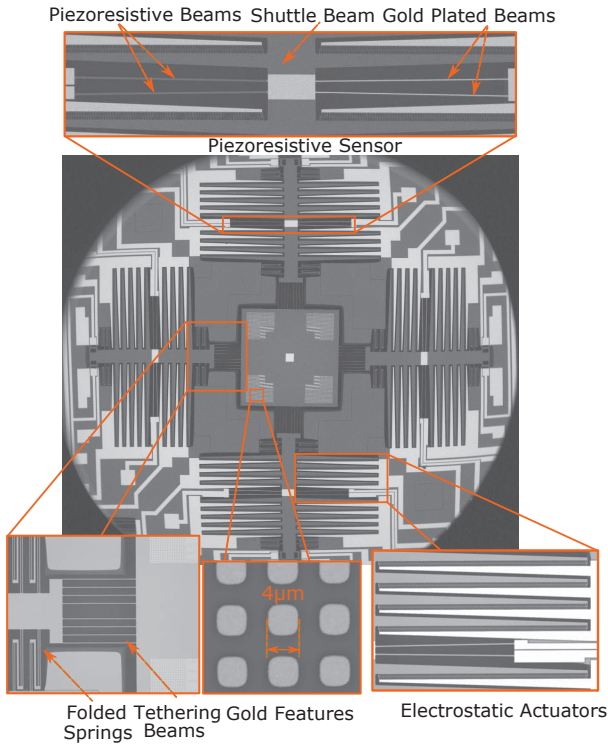


Fig. 1: The SEM image of the MEMS nanopositioner. The close-up views show folded springs and tethering beams, the electrostatic actuators, gold features and the piezoresistive sensor in the Y direction.

TABLE I: The geometrical properties of the proposed MEMS nanopositioner.

Tilted-beam sensors	Normal Length: $h = 1\text{ mm}$	Width: $10\ \mu\text{m}$
	Inclination distance, angle: $\Delta = 15\ \mu\text{m}$ , $\delta = 0.86^\circ$	
Comb finger	Air gap: $2\ \mu\text{m}$	Engagement: $12\ \mu\text{m}$
	Length: $26\ \mu\text{m}$	Width: $2\ \mu\text{m}$
Comb structures	Trapezoidal: Length: $1536\ \mu\text{m}$ , Bases: $20\ \mu\text{m}$ , $75\ \mu\text{m}$	
Shuttle beams	$2443\ \mu\text{m} \times 250\ \mu\text{m}$	
Tethering beams	$500\ \mu\text{m} \times 5\ \mu\text{m}$ , 8 on each side	

characterizations of the nanopositioner show that outputs of the piezoresistive sensors are deemed suitable to be used as measurement in a feedback control loop. An integral resonant controller (IRC) combined with an integral tracking controller are implemented in closed-loop to evaluate the performance of the proposed MEMS nanopositioner in the raster scan [19]. Finally, the controlled nanopositioner is used as a scanner table within a commercially available AFM.

## II. NANOPositioner's DESIGN AND FABRICATION

The scanning electron microscope (SEM) image of the proposed nanopositioner is shown in Fig. 1. A stage with the dimension of  $1.8\text{ mm} \times 1.8\text{ mm}$  is located at the center of the nanopositioner, functioning as the scan table. The nanopositioner has a parallel-kinematic configuration where it is capable of moving bidirectionally along X and Y axes. The device is realized using the standard SOIMUMPs micro

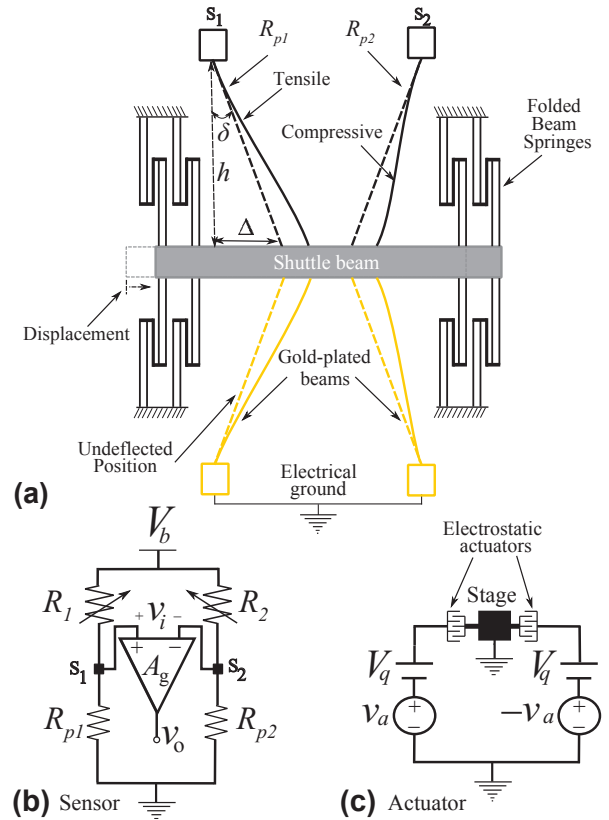


Fig. 2: a) Schematic of the piezoresistive sensor structure when the shuttle beam moves to the right. For the sake of clarity, the deflected shapes of the folded beam springs are not shown. b) The sensing circuit based on Wheatstone bridge. c) Schematic of the actuation circuit.

fabrication process [18]. The process is a silicon-on-insulator MEMS fabrication method with  $25\ \mu\text{m}$  thick single crystal silicon as the device layer. As shown in Fig. 1, square-shaped gold features with the size of  $4\ \mu\text{m} \times 4\ \mu\text{m}$  are also fabricated on the stage to be used as sample patterns for AFM imaging.

Electrostatic comb-drive actuators are implemented on each side of the stage to provide the necessary force. As shown in Fig. 1, the mass of the comb structures is reduced by using of trapezoidal geometry.

To transfer the actuation force to the stage, a shuttle beam is utilized on each side. Tethering beams connect the shuttle beams to the stage, while their lateral compliance allows the stage to move in two orthogonal directions. As part of the mechanical suspension system, eight folded springs are implemented on each side. Each spring comprises two pairs of parallel beams connected to a relatively thick beam in the middle. These folded springs are incorporated instead of the typical clamped-guided beams to achieve a more linear stiffness-displacement behavior [20]. Geometrical properties of the nanopositioner is summarized in Table I.

As clear in Fig. 1, two pairs of tilted beams in a V-shaped configuration are implemented for all shuttle beams functioning as a part of device's suspension system. The close-up view in this figure also shows that the piezoresistive

sensor in each direction comprises two pairs of these tilted beams. The structural configuration of the displacement sensor is further illustrated in Fig. 2a. A pair of the tilted beams is gold plated which constructs a short-circuited path to the electrical ground, while the piezoresistivity of the other pair is used for displacement sensing. Due to the tilted geometry, the displacement of the shuttle beam induces an axial tensile force in one tilted beam and an axial compressive force along the other. These longitudinal forces cause their resistance ( $R_{p1}$  and  $R_{p2}$ ) to change in opposite directions due to the inherent piezoresistivity of silicon [17]. As clear in Fig. 2b, the resistance variations are subsequently converted to a voltage using a Wheatstone bridge and differentially amplified by an instrumentation amplifier at the output.

In [17], this piezoresistive sensor was implemented for a 1-DOF MEMS nanopositioner, where a large feedthrough signal from actuation to sensing was observed. That feedthrough signal limited the sensor's bandwidth to about 8kHz [21]. In the nanopositioner presented here, however, the on-chip signal routing is modified to alleviate the feedthrough signal in the piezoresistive sensors, which dramatically increases their sensing bandwidth.

### III. CHARACTERIZATION

For all experiments, the linear actuation mechanism is implemented for the device in both directions [22]. The actuation circuit is schematically shown in Fig. 2c for one axis, where the actuation voltage designated as  $v_a$  with opposite sign plus a constant dc voltage ( $V_q$ ) are applied to the electrostatic combs. The stage and the moving combs are connected to the electrical ground. Here, the stage experiences a net actuating force which depends linearly on the ( $V_q \times v_a$ ). A 45 V dc bias voltage ( $V_q$  in Fig. 2c) is applied during all tests.

The bias voltage for the sensor in both direction ( $V_b$  in Fig. 2b) is adjusted to 6V. In the absence of the actuation voltage, when the stage is at its equilibrium position, the outputs of the sensors are adjusted to zero using the potentiometers in their readout circuits.

#### A. Static Response

The stage displacement is experimentally measured in both X and Y axes using Polytec MSA-050-3D Micro System Analyzer (MSA). Fig. 3 plots the X and Y displacement of the stage as a function of the actuation voltage ( $v_a$ ). A linear actuation-displacement behavior is observed, where a displacement range of 16  $\mu\text{m}$  and 15  $\mu\text{m}$  are obtained in the X and Y directions, respectively.

The piezoresistive sensors output is also recorded simultaneously and presented in Fig. 3. A linear relationship between sensor outputs and the stage displacement is observable and calibration factors of 0.208 V/ $\mu\text{m}$  and 0.220 V/ $\mu\text{m}$  are obtained for the piezoresistive sensors in X and Y axes, respectively.

A negligible cross coupling (approximately  $-40\text{dB}$ ) is also measured between the two perpendicular axes, which is sufficient to consider the system as two single-input single-output (SISO) systems.

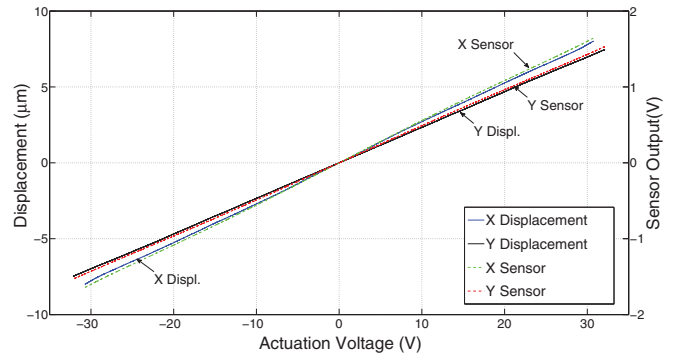


Fig. 3: The displacement of the stage and the piezoresistive sensors output are presented versus actuation voltage ( $v_a$ ) for both directions.

#### B. Dynamic Response

The frequency response of the nanopositioner is also obtained by applying a chirp signal with a bandwidth of 40kHz as  $v_a$  in order to excite the system. The displacement of the stage is directly recorded using the MSA. The frequency responses of the device along the X and Y axes are shown in Fig. 4. The first in-plane frequency occurs at 3626Hz and 3944Hz for the X and Y axes, respectively.

In Fig. 4 the frequency responses of the sensors output are also compared with the system displacement in both axes. For the sake of clarity, the dc gain of the responses are adjusted to unity. As visible, the sensors completely capture the dynamics of the system in a frequency range more than ten times larger than the first mechanical resonant mode in both axes.

The noise at the sensors output is recorded in the time domain sampled at 128 kHz for all sensors within a time duration of 25 s. The resolution of the sensor is 2nm and 1.9nm in the X and Y axes, respectively. The resolution of the sensor is defined as the root mean square (RMS) value of the noise signals which are converted to a displacement resolution using the calibration factors.

The device demonstrates a relatively high-bandwidth with a displacement range more than 15  $\mu\text{m}$  in both axes. In addition, the piezoresistive displacement sensors entirely capture the systems dynamic in a large frequency range without inducing any delay or phase lag. This makes the device favorable for the implementation of various control algorithms. An integral resonant controller (IRC) plus an integral tracking controller are implemented for the device as explained next.

### IV. CONTROLLER IMPLEMENTATION

The performance of the MEMS nanopositioner is evaluated in closed-loop. In order to design a controller, the transfer function of the open-loop plant, from the actuation signal to the sensor output, is initially identified using the least square method [23] as:

$$G_x = \frac{-6.543 \times 10^{-6}s + 0.9773}{1.921 \times 10^{-9}s^2 + 9.101 \times 10^{-7}s + 1}, \quad (1)$$

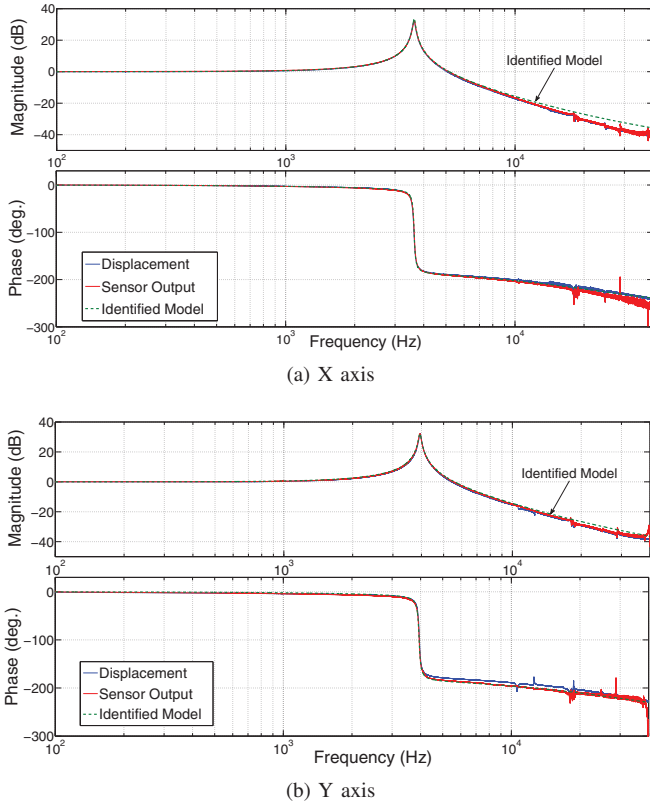


Fig. 4: The frequency response of the MEMS nanopositioner in the X direction (a) and Y direction (b) obtained using the MSA, and piezoresistive sensors in either sides. The frequency response of the identified model (with the unity dc gain) is also compared with the sensor output in both axes.

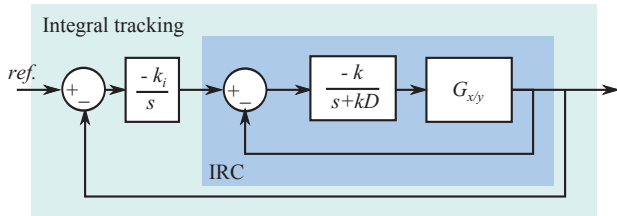


Fig. 5: Schematic of the damping (inner) and tracking (outer) feedback control loops of the MEMS nanopositioner.

$$G_y = \frac{-4.172 \times 10^{-6}s + 0.8818}{1.634 \times 10^{-9}s^2 + 9.965 \times 10^{-7}s + 1}. \quad (2)$$

In Fig. 4, the frequency responses of the identified models are compared with the sensors responses. A close agreement is observable while each second order model ( $G_{x/y}$ ) captures the first resonant mode of the nanopositioner accurately.

As shown in Fig. 5, an IRC is designed and implemented to augment damping to each lateral axis. A high-gain integral control is implemented in the outer feedback loop to provide tracking.

To design IRC, a feedthrough term  $D$  is added to the plant so that  $G_{x/y} + D$  has an interlacing zero-pole pattern rather than the typical pole-zero pattern for lightly damped

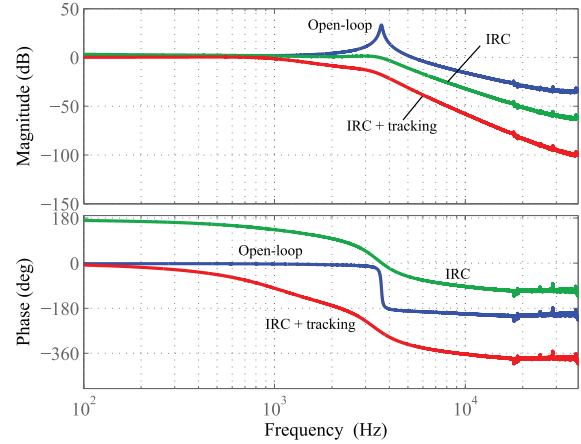


Fig. 6: Measured frequency responses of the MEMS nanopositioning system for open-loop system (blue), closed-loop damped system with IRC (green) and closed-loop system with IRC and integral tracking control (red).

structures. The loop gain of the modified system  $G_{x/y} + D$  is then analyzed in order to find the integral gain  $k$  that provides maximum damping to the system.  $k$  is determined using root-locus plot and the IRC is obtained as:

$$C_{IRC}(s) = \frac{-k}{s+kD} = \frac{-1000}{s+20000}. \quad (3)$$

Since the dominant resonant behavior of the X and Y axes are almost similar, the above IRC can be implemented to both axes. Fig. 6 shows the open- and closed-loop frequency responses of the X axis. The Y axis has similar frequency responses and will not be presented for brevity sake. With the IRC loop in place, the dominant resonant peak was suppressed by approximately 33 dB. This allows a relatively high-gain integral tracking controller to be implemented in the outer loop with gain and phase margins of 13 dB and  $64.5^\circ$ , respectively. The tracking bandwidth of the closed-loop system is 466 Hz.

The step responses of the device in open-loop, in closed-loop with IRC and both IRC and integral tracking controller are compared in Fig. 7. The system shows an under-damped behavior in open-loop with a settling time of approximately 12 ms. The transient behavior of the system is drastically improved with IRC and the settling time is reduced to 3.1 ms. With integral action as the second loop, the settling time is further reduced to 1.3 ms.

Fig. 8 shows the tracking performance of the closed-loop system where the X axis was forced to follow a 25 Hz and 125 Hz triangular references. The RMS tracking error (Error 1 in Fig. 8) at 25 Hz is 170 nm. The error RMS increases to 863 nm at 125 Hz. This is expected as the tracking bandwidth of the closed-loop system reduces at high frequencies, which can also be observed from the frequency response in Fig. 6. A part of this error is simply due to a constant phase lag between the reference signal and closed-loop

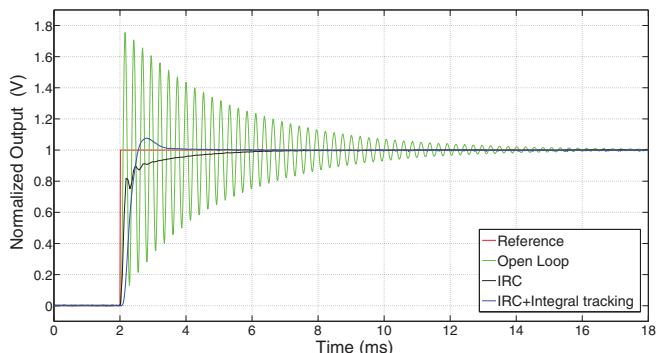


Fig. 7: The step responses of the nanopositioner in open-loop and closed-loop with IRC and IRC plus integral tracking.

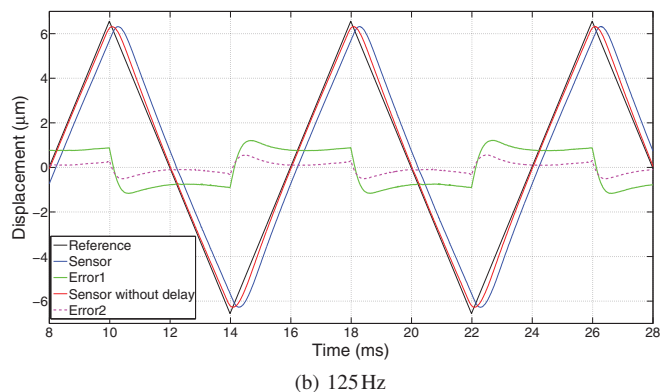
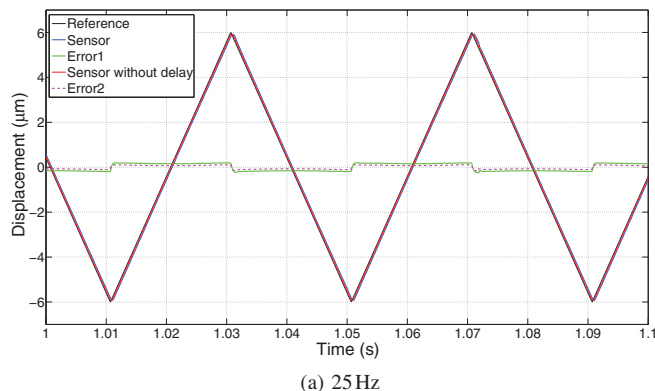


Fig. 8: Tracking performance of the nanopositioner in the X axis. A triangular reference signal with more than  $12 \mu\text{m}$  peak-to-peak displacement is applied.

system output. As visible in Fig. 6, the phase lags are  $1.752^\circ$  and  $8.88^\circ$  for 25 Hz and 125 Hz, respectively. By shifting the sensor signal in time domain according to these phase lags, the RMS values of the error (Error 2 in Fig. 8) decreases to 85 nm for 25 Hz and 256 nm for 125 Hz. The tracking bandwidth can be improved significantly by implementing inversion-based feedforward technique [2], [4], [24].

## V. IMAGING

The proposed nanopositioner is also implemented as the scanning stage within a commercial Nanosurf Easyscan 2 AFM. The AFM's probe is landed on the stage and the

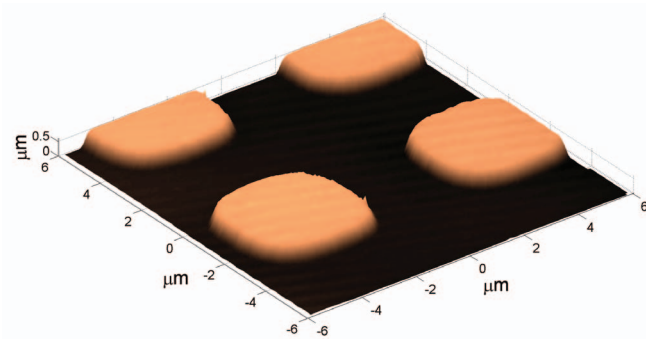


Fig. 9: The AFM image of the features on the stage obtained using raster scan method with the frequency of 25 Hz.

embedded in-plane nanopositioner of the probe within the Nanosurf AFM is bypassed during the tests. The nanopositioner is operated in closed-loop and the imaging is performed via constant-height contact mode. The gold features on the stage are used as the reference pattern. In Fig. 9, an AFM image of the gold features with 520 nm height is shown. The scan is performed in a  $12 \mu\text{m} \times 12 \mu\text{m}$  window, while a triangular signal with 25 Hz frequency is applied to the X axis and the Y axis follows a slow ramp. The tip deflection of the cantilever is measured using the embedded laser sensor of the AFM. The topography of the features is obtained using the piezoresistive sensors and the laser sensor signals as the in-plane position and the features height data, respectively.

## VI. CONCLUSION

A 2-DOF electrostatic MEMS nanopositioner is proposed to be used as a scanner stage in AFM. As the sensing mechanism, the bulk piezoresistivity of tilted clamped-guided beams is exploited and a standard silicon-on-insulator microfabrication process is used for the implementation. The characterization of the device demonstrates displacement range and in-plane resonance modes of above  $15 \mu\text{m}$  and 3.6 kHz, respectively in both axes. The electrostatic combs are actuated linearly and the sensors output shows a linear relation with respect to the stage displacement. The sensors entirely capture the dynamic of the stage in a bandwidth ten times larger than the first mechanical resonance of the device. The linear behavior of the nanopositioner plus the high-bandwidth sensing capability of its sensors make the device promising to be used in different control algorithms. In this study, an IRC together with an integral tracking controller are implemented and a bandwidth of 466 Hz is obtained in closed-loop. The tracking performance of device is tested with a triangular reference signal with an amplitude more than  $6 \mu\text{m}$  with 25 Hz and 125 Hz frequencies and finally, by implementation of raster scan method, the device is used as a scan table for imaging within an AFM.

## REFERENCES

- [1] K. Salaita, Y. Wang, and C. A. Mirkin, "Applications of dip-pen nanolithography," *Nat Nano*, vol. 2, no. 3, pp. 145–155, Mar. 2007.

- [2] S. P. Wadikhaye, Y. K. Yong, and S. O. Reza Moheimani, "A serial-kinematic nanopositioner for high-speed atomic force microscopy," *Review of Scientific Instruments*, vol. 85, no. 105104, 2014.
- [3] E. Eleftheriou, "Nanopositioning for storage applications," *Annual Reviews in Control*, vol. 36, no. 2, pp. 244–254, Dec. 2012.
- [4] M. Maroufi, A. Bazaee, and S. O. R. Moheimani, "A High-Bandwidth MEMS Nanopositioner for On-Chip AFM: Design, Characterization, and Control," *IEEE Transactions on Control Systems Technology*, no. 99, 2014.
- [5] J. Engelen, H. Rothuizen, U. Drechsler, R. Stutz, M. Despont, L. Abelman, and M. Lantz, "A mass-balanced through-wafer electrostatic x/y-scanner for probe data storage," *Microelectronic Engineering*, vol. 86, no. 4-6, pp. 1230 – 1233, 2009.
- [6] N. Yazdi, F. Ayazi, and K. Najafi, "Micromachined inertial sensors," *Proceedings of the IEEE*, vol. 86, no. 8, pp. 1640–1659, 1998.
- [7] A. Mohammadi, A. G. Fowler, Y. K. Yong, and S. O. R. Moheimani, "A Feedback Controlled MEMS Nanopositioner for On-Chip High-Speed AFM," *IEEE Journal of Microelectromechanical Systems*, vol. 23, no. 3, pp. 610–619, 2014.
- [8] Y.-S. Choi, Y. Zhang, and D.-W. Lee, "A thermal-driven silicon micro XY-stage integrated with piezoresistive sensors for nano-positioning," *Journal of Micromechanics and Microengineering*, vol. 22 (055002), no. 5, 2012.
- [9] B. Koo, X. Zhang, J. Dong, S. Salapaka, and P. Ferreira, "A 2 Degree-of-Freedom SOI-MEMS Translation Stage With Closed-Loop Positioning," *Journal of Microelectromechanical Systems*, vol. 21, no. 1, pp. 13–22, 2012.
- [10] J. Dong and P. M. Ferreira, "Simultaneous actuation and displacement sensing for electrostatic drives," *Journal of Micromechanics and Microengineering*, vol. 18 (035011), no. 3, 2008.
- [11] L. L. Chu and Y. B. Gianchandani, "A micromachined 2D positioner with electrothermal actuation and sub-nanometer capacitive sensing," *Journal of Micromechanics and Microengineering*, vol. 13, no. 2, p. 279, 2003.
- [12] B. Boser, "Electronics for micromachined inertial sensors," in *International Conference on Solid State Sensors and Actuators, 1997. TRANSDUCERS '97 Chicago*, vol. 2, 1997, pp. 1169–1172 vol.2.
- [13] M. A. Lantz, G. K. Binnig, M. Despont, and U. Drechsler, "A micromechanical thermal displacement sensor with nanometre resolution," *Nanotechnology*, vol. 16 1089, no. 8, 2005.
- [14] B. Krijnen, R. P. Hogervorst, J. W. van Dijk, J. B. C. Engelen, L. A. Woldering, D. M. Brouwer, L. Abelman, and H. M. J. R. Soemers, "A single-mask thermal displacement sensor in MEMS," *Journal of Micromechanics and Microengineering*, vol. 21 074007, no. 7, 2011.
- [15] M. Maroufi, A. G. Fowler, A. Bazaee, and S. O. R. Moheimani, "High-stroke silicon-on-insulator MEMS nanopositioner: Control design for non-raster scan atomic force microscopy," *Review of Scientific Instruments*, vol. 86, p. 023705, 2015.
- [16] E. Guliyev, B. E. Volland, Y. Sarov, T. Ivanov, M. Klukowski, E. Manske, and I. W. Rangelow, "Quasi-monolithic integration of silicon-MEMS with piezoelectric actuators for high-speed non-contact atomic force microscopy," *Measurement Science and Technology*, vol. 23 074012, no. 7, 2012.
- [17] A. Bazaee, M. Maroufi, A. Mohammadi, and S. Moheimani, "Displacement Sensing With Silicon Flexures in MEMS Nanopositioners," *Journal of Microelectromechanical Systems*, vol. 23, no. 3, pp. 502–504, 2014.
- [18] A. Cowen, G. Hames, D. Monk, S. Wilcenski, and B. Hardy, *SOI-MUMPs Design Handbook, Revision 8.0*, MEMSCAP Inc., 2011.
- [19] B. Bhikkaji and S. Moheimani, "Integral Resonant Control of a Piezoelectric Tube Actuator for Fast Nanoscale Positioning," *IEEE/ASME Transactions on Mechatronics*, vol. 13, no. 5, pp. 530–537, 2008.
- [20] R. Legtenberg, A. W. Groeneveld, and M. Elwenspoek, "Comb-drive actuators for large displacements," *Journal of Micromechanics and Microengineering*, vol. 6, no. 3, pp. 320–329, 1996.
- [21] M. Maroufi, A. Bazaee, A. Mohammadi, and S. O. Reza Moheimani, "Tilted Beam Piezoresistive Displacement Sensor: Design, Modeling, and Characterization," *Journal of Microelectromechanical Systems*, 2015. [Online]. Available: <http://dx.doi.org/10.1109/JMEMS.2015.2426180>
- [22] M. Maroufi and S. O. R. Moheimani, "Design, Fabrication and Characterization of a High-Bandwidth 2DOF MEMS Nanopositioner," in *IEEE/ASME International Conference on Advanced Intelligent Mechatronics*, Wollongong, Australia, July 2013, pp. 335 – 340.
- [23] M. A. Soderstrand, G. Berchin, and R. S. Roberts, "Frequency domain least squares system identification," *International Journal of Electronics*, vol. 78, no. 1, pp. 25–35, 1995.
- [24] Y. Yong, S. S. Aphale, and S. O. R. Moheimani, "Design, Identification, and Control of a Flexure-Based XY Stage for Fast Nanoscale Positioning," *IEEE Transactions on Nanotechnology*, vol. 8, no. 1, pp. 46–54, 2009.